5770

NASA Technical Memorandum

NASA TM-86547

SURFACE FILM EFFECTS ON DROP TUBE UNDERCOOLING STUDIES

Center Director's Discretionary Fund Final Report

By E. C. Ethridge and W. F. Kaukler

Space Science Laboratory
Science and Engineering Directorate

April 1986

National Aeronautics and Space Administration

George C. Marshall Space Flight Center

ND736 801

TECHNICAL REPORT STANDARD TITLE PAGE

1. REPORT NO.	2. GOVERNMENT ACCESSION NO.	3. RECIPIENT'S CATALOG NO.
NASA TM-86547		

4. TITLE AND SUBTITLE	5. REPORT DATE
Surface Film Effects on Drop Tube Undercooling Studies – Center Director's Discretionary Fund Final Report	April 1986
	6. PERFORMING ORGANIZATION CODE

7. AUTHOR(S)	8. PERFORMING ORGANIZATION REPORT #
E. C. Ethridge and W. F. Kaukler*	

9. PERFORMING ORGANIZATION NAME AND ADDRESS	10. WORK UNIT NO.
George C. Marshall Space Flight Center Marshall Space Flight Center, Alabama 35812	11. CONTRACT OR GRANT NO.
	13. TYPE OF REPORT & PERIOD COVERED
12. SPONSORING AGENCY NAME AND ADDRESS	Technical Memorandum
National Aeronautics and Space Administration Washington, D.C. 20546	14. SPONSORING AGENCY CODE

15. SUPPLEMENTARY NOTES

Prepared by Space Science Laboratory, Science and Engineering Directorate. AM-86405
*Chemistry Department, University of Alabama in Huntsville, Huntsville, AL 35899.

16. ABSTRACT

The effects of various gaseous atmospheric constituents on drop-tube solidified samples of elemental metals were examined from a microstructural standpoint. All specimens were prepared from the purest available elements, so effects of impurities should not account for the observed effects. The drop-tube gas has a definite effect on the sample microstructure. Most dramatically, the sample cooling rate is affected. Some samples receive sufficient cooling to solidify in free fall while others do not, splating at the end of the drop tube in the sample catcher. Gases are selectively absorbed into the sample. Upon solidification gas can become less soluble and as a result forms voids within the sample. The general oxidation/reduction characteristics of the gas also affect sample microstructures.

In general, under the more favorable experimental conditions including reducing atmospheric conditions and superheatings, examination of sample microstructures indicates that nucleation has been suppressed. This is indicated by underlying uniform dendrite spacings throughout the sample and with a single dendrite orientation through most of the sample. The samples annealed yielding a few large grains and single or "bi-crystal" samples were commonly formed. This was especially true of samples that were inadvertently greatly superheated. This is in contrast with results from a previous study in which surface oxides were stable and contained numerous sites of nucleation. The number of nucleation events depends upon the surface state of the specimen as determined by the atmosphere and is consistent with theoretical expectations based upon the thermodynamic stability of surface oxide films. Oxide-free specimens are characterized by shiny surfaces, with no observable features under the scanning electron microscope at 5000X.

17. KEY WORDS	18. DISTRIBUTION STATEMENT
Drop Tube Undercooling Nucleation Elemental Metals	Unclassified – Unlimited

19. SECURITY CLASSIF. (of this report)	20. SECURITY CLASSIF. (of this page)	21. NO. OF PAGES	22. PRICE
Unclassified	Unclassified	36	NTIS

MSFC - Form 3292 (May 1969)

ACKNOWLEDGMENTS

The authors would like to thank Dr. Gary Workman and his staff at UAH for their assistance in the drop tube experiment implementation and Donna Warden for much of the metallographic polishing of the samples.

TABLE OF CONTENTS

LIST OF ILLUSTRATIONS

TECHNICAL MEMORANDUM

SURFACE FILM EFFECTS ON DROP-TUBE UNDERCOOLING STUDIES

Center Director's Discretionary Fund Final Report

INTRODUCTION

One major emphasis of the Materials Processing in Space program is the containerless processing and solidification of materials. It has been demonstrated that the absence of surface effects from containers during cooling allows bulk melts of some metals to be lowered far below the thermodynamic melting temperature prior to solidification. In other Marshall Space Flight Center (MSFC) drop-tube studies, molten Pd-Si-Cu has been successfully undercooled in bulk droplets to the glassy state [1]. Alloys of Nb-Ge and Nb have been undercooled by 500°C and 525°C, respectively [2,3]. Other tested materials such as Cu-Zr and Ni-3Al do not seem to exhibit this propensity to undercool significantly [4]. It is believed that surface oxidation plays a significant role in heterogeneous nucleation. Drop tube experimentation offers the advantage of containerless solidification in the absence of certain nucleation effects so that the effect of surface films upon nucleation can be examined.

An objective of this study was to further the understanding of the role of surface effects during solidification of pure metals and alloys in the MSFC drop tube and to aid the understanding of heterogeneous nucleation effects. This should allow one to optimize the use of drop tubes to conduct undercooling nucleation and rapid solidification studies of metals. The approach was to containerlessly melt the samples at the top of the drop tube, drop the molten samples down the tube through gases with different partial pressures of reactant gas, and solidify containerlessly during freefall. Metallographic analysis of the samples reveals information about the sample solidification history.

THEORY

Oxidation-Reduction

The stability of a metal with relation to its oxide at various temperature is commonly represented on a plot of the free energy versus temperature. The position of a reaction curve on the plot is indicative of the metal's reactivity with oxygen. An application of the thermodynamic relationship between free energy, temperature, and oxygen partial pressure is that one can plot free energy as a function of temperature for any partial pressure on the same graph with metal oxidation. Utilizing this data one can determine oxide stability in terms of temperature and oxygen partial pressure. Existing published figures contain metals of interest to the particular discipline of each author. Several of the elements used in this study do not commonly appear in the published literature. It was, therefore, necessary to calculate and plot this data for elements used in this study.

The method described by Richardson and Jeffes [5] was utilized with thermodynamic data from common references [6]. Free energy versus temperature data were

directly plotted for common reactions. Less common reactions required the use of standard state enthalpy and entropy data along with specific heat versus temperature data to calculate the free energy at a given temperature with the Gibbs-Helmholtz equation.

Pendant Drops

When the end of a wire such as with an electron beam furnace is melted, a certain amount of liquid will remain on the wire without dropping. Further melting will cause the drop to pull away and break off due to gravity. Tate's law is a simple relation that describes the mass of the molten drop with the liquid surface tension (dyne/cm) and predicts when a drop will fall [7]. Tate's law is expressed as,

$$mg = 2 \pi r \nu \quad , \tag{1}$$

where m is the drop mass, g is gravitational acceleration, r is the wire radius, and ν is the surface tension. Tate's law calculations were used as a first approximation for the determination of the amount of wire to be used in the electron beam furnace experiments. Table I shows the properties of metals melted by electron beam melting and the calculated critical drop mass and length of wire to form the critical drop for two different sample wire diameters.

EXPERIMENTAL PROCEDURE

Sample Preparation

Seven elemental metals including Cu, Pd, Ni, Rh, Ir, Pt, and Re were selected for the instability of their surface oxides. Depending on the starting form of the material and the processing technique, different sample preparation techniques were used. All the samples were cleaned prior to melting in the drop tube. The cleaning procedure included washing in acetone and/or alcohol, rinsing with deionized water, soaking in 33 percent HF acid, final rinsing with ethanol, and packaging in plastic containers. Samples to be melted in the electromagnetic (EM) levitation furnace need to be close to spherical in shape in order to facilitate processing. The Ni samples were prepared by arc melting a preweighed piece of high-purity wire into a roughly spherical sample. These samples were cleaned and weighed prior to processing in the EM levitator. Cu and Pd samples were cut from large wire stock to form cylindrical samples. Different diameter wires as received were used for the electron beam furnace melting techniques.

In the MSFC drop tube the samples were levitated (or suspended in the case of electron beam melted samples), melted, and then dropped in free fall down the 20-cm-diameter, 105-m-long drop tube through a controlled atmosphere (Fig. 1). Each sample was retrieved after the drop, visually examined, photographed with an enlarging camera, and many were examined with scanning electron microscopy to examine for surface morphological effects. All samples were mounted, mechanically ground, polished, etched, and micrographically examined with a metallograph.

Drop-Tube Experiments

Drop-tube solidification is a technique that allows the melting and solidification of a sample in a totally containerless environment. Most metals can be levitation-melted in a gas (or vacuum) atmosphere using electromagnetic induction levitation melting. Electron beam melting of wires can also be utilized for materials that are difficult to levitate or for refractory metals that are hard to melt, but this process requires the use of a good vacuum since a tungsten filament is used.

Samples processed in a vacuum cool primarily by radiation. In general, lower melting temperature metals were melted (by electromagnetic induction levitation) so that they could be dropped through a quench gas in order to achieve sufficient cooling rates for solidification. A number of higher melting elements were processed in the electron beam furnace. In the electron beam furnace, a tungstem filament is heated to incandescence by resistance heating. A 40-kV potential is set up on the filament and the sample to be heated is held at ground potential. Electrons flow from the filament to the sample by thermionic emission and the sample (wire) is heated by joule heating.

A 15-kW Lepel RF generator was used for the containerless electromagnetic levitation studies. Coils were prepared by winding against a split mandrel in a special jig [8]. The output coil tap in the RF generator was selected to get the optimum levitation. This setting was satisfactory for any given coil design. For controlled heating of the sample, the power control was adjusted. Sample processing was started by turning the power to about 60 percent giving a reading of about 6.2 kV on the plate of the power tube causing samples to levitate. To further heat the samples, the power would be reduced to allow the sample to move down into the conical-shaped coil where closer coupling to the windings was achieved. Typically, 150 to 400 mg samples were levitated and melted with this procedure.

Environmental gaseous conditions for the studies included high-purity He, He-6%H, high-purity Ar, air, and vacuum (10^{-5} torr). The samples were processed in gas pressures ranging from 200 to 760 torr.

Numerous drop tube experiments were performed. In the first phase of the study, electron beam melting of refractory elements Re, Rh, and Ir in vacuum was performed. It was not possible to acheive any control over environmental gaseous conditions in the vacuum. For the second phase, radio frequency EM induction levitation and melting in various atmospheres was utilized to continue the studies. Over 150 drop tube experiments were attempted resulting in over 60 melted samples for analysis (Table II). The three elemental metals, Pd and Ni (from group VIII) and Cu (from group IB) provide the bulk of the data. Samples with weights ranging from 150 to 400 mg were used in order to vary the effective cooling rate.

Pyrometer Data

A single-color optical pyrometer made by the Pyrometer Instrument Co. was used at the top of the drop tube to measure the temperatures of electromagnetically levitated samples while levitated. It measured the temperature of the sample from directly above the sample through a fused silica window in the cover over the bell jar feedthrough ring. The pyrometer was not used with the pendant drops melted by the electron beam furnace since these samples are close to the melting temperature and the experimental setup prevented its use.

Three silicon photovoltaic detectors are installed in the drop tube at 1, 50, and 83 m to detect recalescence. Data at the rate of 5,000 readings per sec were taken for each successful drop using a Hewlett Packard data acquisition system and HP 9835 microcomputer. In some cases computer or operator malfunctions prevented the collection of recalescence data. About 30 cooling curves were obtained for Cu, Ni, Pd, Rh, and Pt samples. In no case was a recalescence peak observed. This is in part due to the low sensitivity of the Si detectors' detectivity to the radiation from these relatively low temperature samples. Detection of recalescence would have been possible only if it occurred within the first 0.5 sec near the first detector or between 2.8 to 3.0 sec shortly after passing the second detector. The third detector at about 4.2 sec of free fall never detected the sample unless the sample splatted at the bottom of the drop tube (Fig. 2).

Metallography

Over 60 drop tube specimens were mounted, ground, polished, and analyzed metallographically. Some specimens revealed microstructural details on their exterior surfaces. These specimens were examined by scanning electron microscopy and optical metallography prior to mounting and sectioning. Practically all the experimental results are derived from these metallographic studies. Microstructural correlations to the drop tube conditions are the most important observations.

The drop tube specimens ranged in size from 20 to 400 mg. The smaller ones were from electron beam melting, whereas the larger samples came from electromagnetic levitation experiments. The very tiny samples presented considerable difficulty during handling and mounting, and, in particular, during polishing. There was a tendency for the samples to "pop out" of the sample mount. Nearly all of the specimens were spheres so that microscopy of features on the surface was extremely difficult to obtain.

All the specimens were mounted in standard 1.25-in.-diameter specimen mounts with cast polymethyl methacrylate "cold mount" for handling during polishing. They were ground with SiC paper using water as the lubricant through the sequence 120, 180, 230, 420, and 600 grit paper. Polishing was then accomplished with suspended alumina polishing media of 5, 1, and 0.3 μm particle size. During coarse polishing, Buehler "super finale" cloth was used followed with "billiard cloth" for the final polish. With some samples, diamond abrasives of 1 and 0.25 μm particle sizes suspended in a polishing oil on a "Rayvel" cloth were used for the final polish. With copper samples after mechanical polishing, a chemical polish was used to remove the residual surface scratches.

Much time was spent on the development of the various metallographic techniques required to produce usable micrographs of these pure elemental samples. Many of the samples were soft and, therefore, scratched very easily. They also were easily deformed during polishing, became rounded around the edges, and became embedded with grinding and polishing abrasives in the surface. To alleviate some of the problems a ring of glass was embedded with the sample to improve the polishing characteristics.

Each of the metals required its own etching techniques. Many were tried from the literature but some of the successful ones were developed during this study. Since the samples in this study are of very high purity and some are noble metals, metallographic preparation is difficult since features of the microstructure are much

more difficult to enhance and delineate. Both chemical and electrochemical etching of samples was utilized. If chemical etchants were not immediately successful, then electrochemical techniques were used. The high nobility of some of the metals required aggressive techniques for etching.

The chemical polish for copper [9] was composed of 30 ml nitric acid, 10 ml hydrochloric acid, 10 ml phosphoric acid, and 50 ml glacial acetic acid. The process consisted of submerging the specimen in the solution for several seconds at a time, rinsing, and then examining for scratches. The process was repeated until no scratches remained. The copper samples were etched immediately after the chemical polish. The most readily available etchant was a diluted (10 percent) mixture of commercial printed circuit board etchant (ferric chloride) in water. A few seconds of immersion at room temperature was sufficient to reveal both the recrystallized grains and the underlying dendritic structures.

Etching of Ni [9] utilized a fresh mixture of 50 percent nitric acid and 50 percent glacial acetic acid for 5 to 30 sec at room temperature. This published procedure was most useful.

The chemical etch for palladium was difficult to develop. It was learned that palladium could be etched with a 5 to 10 percent dilution of chromic/sulfuric acid, a commercial glass cleaning solution. The etch time was from 30 sec to 1 min.

The three noble metals Pt, Rh, and Ir were electrochemically etched with a solution consisting of 20 ml hydrochloric acid and 25 g of sodium chloride in 65 ml of distilled water. The solution was used at room temperature with constant stirring to remove bubbles formed during the reaction. An electropolishing setup was constructed as shown in Figures 3 and 4. The sample was attached to one electrode and a rod of graphite was used as the second electrode. An a.c. potential of 6 V between the electrodes resulted in good results. With Rh, as much as 2 min of etching was required. With Pt, however, 20 sec was usually sufficient to highlight the microstructure.

With all the etchings, the sample was rinsed, between treatments, in water, in alcohol, and then dried with clean pressurized air. Considerable rinsing was required to prevent acid trapped in porosity from bleeding out and subsequently attacking the surface, destroying the etch.

Photomicrography

Metallographic examination of the specimens combined exterior observation by optical and electron microscopy with micrography of the polished and etched sections. The sample features examined included dendrite size and spacings, surface oxidation, grain size, porosity, and sites of nucleation if possible. The dimensions of these features are such that only low magnifications are needed.

A Zeiss Ultraphot Research Microscope and a Unitron U-11 metallograph were used for optical metallography. A JEOL UM-3 scanning electron microscope was also used for surface examination. Several special lighting techniques available on the Zeiss microscope were used to enhance the contrast for the very rough structures sometimes seen due to solidification shrinkage in interdendritic cavities. During light microscopy Kohler, i.e., bright field, illumination was used in most cases; but,

occasionally, when unetched specimens were examined, Nomarski interference contrast illumination was utilized to reveal the subtle variations in surface texture. Surface examination by optical photomicrography was accomplished using dark field illumination on the Zeiss microscope.

Three objective lenses were used yielding three magnifications for the micrographs. These are shown in Table III. Only Kohler illumination was available with the Unitron U-11 and all micrographs were taken with the 10X objective, resulting in a 136.5X magnification on the micrographs. When photographs were taken with the Zeiss microscope, either Polaroid type 58 (for color) or 57 (for black and white) film was used; whereas with the Unitron, Polaroid type 108 or 107 file was used.

Residual Gas Analysis Techniques

Knowledge of the constitution of the atmosphere in the drop-tube environment was critical to the project. The partial pressures of the significant gaseous species such as oxygen, water, hydrogen, carbon monoxide, helium, and carbon dioxide collectively control the chemical potential for reaction at the elevated temperatures used with the specimens. Either oxidation or reduction of the metal could result during its melting and fall through the atmosphere within the tube, depending on the gas selection and sample temperature. Even a high vacuum could contain enough oxygen or water to cause some oxidation of the metal at the temperatures involved. Quantification of the amount of these gases can only be performed with a quadrupole mass spectrometer.

A new Dycor Electronics M/100M series unit was used for this application. The unit was installed onto the bell jar at the top of the tube, above the isolation valve. This unit has a mass range of 1 to 100 amu and is outfitted with an electron multiplier for very sensitive measurements at very low partial pressures. All the spectra are presented in bar graph form with an accompanying tabular set of calculated gas partial pressures. The spectra are within the 1 to 50 amu mass range. The electron multiplier was not used since the gas partial pressures were sufficiently high. The unit has preprogrammed computer-controlled measurement, scaling, calculation of partial pressures, and display of selected gas data. All the spectra represented here were printed by this unit on its own dot matrix printer.

The valving of the mass spectrometer and the vacuum system permits various operations to be performed. Under normal operating conditions, the two valves which bracket the mass spectrometer system, one at the turbomolecular pump (TMP) end and the other at the bell jar, are closed. After normal pumping to 100 μm of Hg with the roughing pump, the turbomolecular pump can be opened to the bell jar via a large isolation valve. Only after the overall pressure is in the 10^{-4} range was the mass spectrometer reopened to the turbomolecular pump and/or the bell jar. With this arrangement the mass spectrometer can analyze the partial pressures of the gases in the vacuum chamber.

A calibrated digital leak metering valve was used to sample the gas in the bell jar where the overall pressure was greater than the 10^{-4} maximum pressure limit of the mass spectrometer. When a cooling gas such as high-purity He, He-H mixture, or other atmospheres other than vacuum were utilized, this metering valve permitted the controlled sampling of the gas in order to determine its composition by mass spectrometry analysis. Although pure He may have been backfilled into the tube to a pressure of 200 torr, a good vacuum was required for the mass spectrometer.

Even with the best vacuum, significant partial pressures of oxygen and water are present. Sampling the drop-tube gas through the metering valve merely dilutes these background gases and reduces their partial pressures. These partial pressures of oxidizing gases need to be known in order to determine the presence of oxide and the potential for it to form based on the Ellingham diagram data.

RESULTS AND DISCUSSION

Oxidation-Reduction Calculations

A computer program was completed that calculates and plots, for a given metal, the free energy versus temperature from reference data. These data are shown in Figure 6. Superimposed on these plots are oxide stability curves calculated for various oxygen partial pressures and with specific hydrogen gas-to-water vapor partial pressure ratios in the atmosphere. These calculations using free energy of formation data for oxides have been used to generate working curves to determine, under various conditions of low oxygen partial pressures, which oxides if any are stable and which are effective for stripping surface oxides from some metals. A series of working curves have been drawn for estimating the atmospheric conditions in the drop tube and for correlation with metallographic results in this study. It can also aid potential drop tube users in predicting when surface reaction films are expected to form.

Drop Tube Experiments

As stated earlier over 60 drops were made of Cu, Pd, Ni, Rh, Pt, and Ir. The electron beam melting experiments in vacuum were not very successful. It was difficult to melt sufficient material and make drops from the suspended wire technique. Attempting to melt a bundle of wire of suitable size was, in general, also unsuccessful. Sometimes the supporting wire melted, dropping the unmelted or partially melted sample. There were too few successful samples to draw definite conclusions.

The bulk of useful experiments was from electromagnetic levitation melted samples. Molten drops processed in vacuum all splat at the end of the drop tube and will not be discussed further in this paper. The three environmental conditions that yielded information are air, He, and H-He. In air and for He (with 10 to 100 ppm of oxygen contamination), the processing of Cu and Ni is favorable for oxidation of the sample at the elevated processing conditions. Pd, on the other hand, is reduced under these same conditions. Experiments in 200 torr He-H are all favorable for the reduction of surface oxides for all three elements.

An observation from these drop tube experiments was that even under conditions favorable for oxide reduction, some samples were visibly oxidized. This could be due to a number of reasons. The vacuum system is very complex with many fittings and seals. Vacuum leaks have been a continuing problem with drop tube experiments prior to and during this study. The system is not baked out so adsorbed water vapor is present and can outgas into the vacuum. Either of these factors can act to greatly affect the environmental conditions of an experiment. The best practical steps were taken to minimize these problems, including backfilling with an inert gas prior to opening to air, rapidly inserting new samples to minimize exposure to normal atmosphere, and keeping the system pumped down when not in use.

In a few experiments, the optical pyrometer, used to monitor sample temperatures while levitated, malfunctioned. This gave temperature readings too low. These samples are labeled as "not completely melted" in Table II; in fact they were superheated by unknown amounts. As will be discussed later, these same samples yielded unusual single or "bi-crystal" microstructures.

Mass Spectrometry

A Dycor quadrupole mass spectrometer was used to examine the background gases present in the drop tube bell jar. The data were plotted in a bar graph mode as partial pressure versus mass unit. The most effectively ionized gas species were selected for printing of the pressure values. These included O_2^+, N_2^+, CO_2^+, Ar^+, He^+, H^+, OH^+, and H_2O^+. A summary of mass spectrometry measurements is reported here. The measurements were made for atmospheric conditions which simulated the conditions of drop tube experiments; namely, for a vacuum, air, and 200 torr He-5%H.

Mass spectrometry data for three separate measurements of the vacuum conditions of the drop tube bell jar are shown in Figure 6. The times of these measurements are the start of one day after pumping all night (Fig. 6a), and shortly after backfilling with He-H and pumping to a good vacuum (Figs. 6b-c). As can be seen in the figure, the water peak is lower after pumping all night than it is after opening the chamber, backfilling, and pumping to about the same vacuum level. The ratio of H_2:H_2O is important from an oxidation-reduction standpoint. This ratio ranges from 0.07 to 0.4 and is shown in Figure 5. Likewise, the total oxygen pressure ($O^+ + O_2^+$) is also very important and is also shown in the figure.

During electron beam melting, the hot tungsten filament has the potential of heating furnace components resulting in outgassing. It may also potentially interact with the background gases affecting the partial pressures of the gases. Figure 7 shows mass spectrometry data before (Fig. 7a) and after (Fig. 7b) the electron beam was turned on for 5 min. Outgassing due to heating of various furnace components increases the total pressure, and selectively increases the partial pressure of N_2^+ and O_2^+. The total pressure of hydrogen ($H^+ + H_2^+$), the total water pressure ($OH^+ + H_2O^+$), and the total oxygen pressure ($O^+ + O_2^+$) were approximately constant. This indicates that there is no reaction between the tungsten and gas species and is consistent with the constructed Ellingham diagram. There was an unexpected relatively large decrease in the mono-atomic C, N, and F peaks. This is unexplained at this time.

For conditions other than vacuum, the metering valve system was needed to sample the gases in the jar so that the mass spectrometer could accept them for measurement. Figure 8 illustrates mass spectrometry data from three different micrometering valve settings with 200 torr He-H gas in the bell jar. As can be seen in Figure 8, the relative ratio of H_2:H_2O increases as the metering valve is adjusted from relative settings of 0, 50, and 125. This indicates that as more gas is leaked into the mass spectrometer line, the relative heights of the leaking gas increase, but background pressures of certain species such as H_2O can be much larger than the gas being sampled. It is, therefore, difficult to extract the small difference from the large background signal. The H_2:H_2O ratio cannot be determined from mass spectrometry data using the present arrangement.

One can calculate the approximate theoretical ratio of H_2:H_2O from the starting gas. It is known that the concentration of H_2 in the gas is about 5 percent. Since the mixture was water-pumped at the filling station, the concentration of water in the mixture can be as high as 20 ppm. This gives a H_2:H_2O ratio of 2.5×10^{-5}. The gas was run through a cold trap and/or gettering furnace to remove water and oxygen so the ratio has to be greater than this but much less than the 1.3 measured by partial pressure ratios in the mass spectrographs. This boundary region is also shown in Figure 6.

In operation, the metering valve permitted a controlled leak of the bell jar through the mass spectrometer into the TMP. This arrangement allows the analysis of the residual gases above the background levels established by the TMP vacuum level. A better arrangement is planned for future installation, where a cryogenic pump dedicated to the mass spectrometer can significantly reduce this background. Insufficient time prevented its installation during this study.

Data for a typical mass spectrum of a sample of air along with the typical composition of air obtained from a CRC chemistry Handbook are shown in Table IV. These data indicate that the pressure measured by the mass spectrometer is not directly proportional to the gas level in air. This is due to three possible causes. Vacuum pumps are not as efficient at pumping all gas species, the metering valve is selectively porous for different gases, and the gas species are not equally ionized. Also, the water vapor originally present could ultimately be detected as the total of two species, OH^+ and H_2O^+.

The partial pressure of water present in the atmosphere can vary over a large range. On a dry winter day (5 percent humidity, 23°F) the partial pressure could be as low as 0.2 torr, while on a hot humid summer day (100 percent humidity, 95°F) it could be as high as 43 torr. Assuming equal vacuum pumping rates for all gas species, the ratio of H_2:H_2O would be in the range of 5×10^{-4} to 1×10^{-3}.

Dissolved Gases

Redox reactions and the resulting oxides are not the only gas-related effects on the microstructure. During the examination of specimen sections, fine dispersions of porosity were found within many of the samples. The morphology of these pores indicates that they formed as a result of the nucleation of dissolved gas throughout the melt upon cooling. Many specimens show that these pores formed in the interdendritic liquid that was last to freeze. The porosity often outlined the interdendritic regions and thus proves that they resulted from the segregation or partitioning effects of the advancing solidification front (Figs. 9, 10, and 11).

A survey of the data for gas solubility was performed in order to determine the most likely candidate for the porosity. The stability of the oxide does not indicate lack of solubility of the oxygen in the melt. For porosity to occur, the solubility in the solid should be significantly lower than in the melt. In addition, adequate gas partial pressures would be needed to cause the dissolution of the gas into the liquid metal. The small droplet sizes with their high surface-to-volume ratio and the high temperatures aid gas dissolution into the samples.

The noble gases He and Ar do not dissolve in any metal to a measurable degree [10]. Three elemental gases can be considered to be likely to cause the observed porosity: H_2, N_2, and O_2. Oxygen and hydrogen may arise not only from background gas partial pressures but also from dissociated water that was always present in the drop tube atmosphere. These solubility data are summarized in Table V. In general, nitrogen is insoluble in these metals and cannot be the cause for porosity in all cases.

Sievert's solubility law applies with hydrogen, in that the solubility is proportional to the partial pressure. Given that no more than 5 percent H_2 was present in the helium mixture and considering that the overall pressure was around 200 to 300 torr, the partial pressure of hydrogen was 0.01 to 0.02 torr. These low hydrogen partial pressures were confirmed with mass spectrometry measurements. The high solubility of hydrogen in Pd at 760 torr (0.7 a/o) is reduced to 0.0001 a/o. Similarily, the solubility of hydrogen in liquid Cu would be 5×10^{-6} a/o for the partial pressures in the tube with the He-H mixture. It is unlikely that hydrogen was dissolved into the liquid melts.

Since porosity was observed mostly in the Ni and Pd samples processed in air as well as some Ni samples processed in He-H, it is a fair conclusion that the dissolved gas is oxygen. This oxygen came from the atmosphere or from oxide originally present in the metal or on the sample surface.

Microscopy

A large number of microstructure types were obtained with drop tube experiments. Upon first examination, some structures appeared to have large equiaxed grains, while other, very similar samples had dendritic structures with fine dendrite arm spacings. Figure 9 illustrates the effect of cooling rate and mode of solidification on the resulting microstructure of Pd. Samples dropped in the reducing environment of H-He had large equiaxed grains. The presence of the annealed structure was not immediately understandable until samples that partially solidified in the drop tube were examined (Fig. 9). These splatted samples exhibit dendritic structures with the smaller (faster cooling) samples having the smallest dendrite spacings.

For the samples that completely solidified the latent heat of fusion is released during solidification, reheating the sample. This heat is sufficient to anneal the structure, thereby masking the original solidification microstructure. The grain size of these annealed samples increased with increasing sample size scaling with cooling rate, i.e., those that cool slower can anneal longer. Samples that were molten or only partly solidified at the end of the drop tube splatted at the bottom. Molten liquid was then available to wet the splat surface, providing an efficient thermal coupling to the cold drop tube structure, effectively dissipating the heat, and preventing the sample from annealing. In a number of other drops, there were splats of completely molten samples. These gave no useful information.

With diligent effort including repeated repolishing and re-etching, one can reveal the underlying dendritic structure in the annealed samples. This is illustrated for Ni, Pd, and Cu in Figure 10. The dissolved gas present in the molten metal sometimes precipitates from solution and manifests itself as porosity at the interdendritic spaces. This is well illustrated in Figure 11.

Determination of the nucleation mechanism for solidification is very difficult. In a rare case for a sample of Cu that was solidified in the reducing H-He gas mixture, it appears that solidification nucleated on the sample surface behind the field of view, as indicated in Figure 12. This sample partially solidified in free fall with the remaining liquid splatting at the bottom of the drop tube. The splatted portion of the sample has the fine grain structure at the bottom of the composite picture. The solidification that took place while in free fall is marked by the larger grains in the upper portion of Figure 12. The initial metal to solidify is undercooled and the spacing of the initial dendrites (or grains) to solidify are small. As solidification proceeds the release of the latent heat of fusion reheats the sample, causing the spacings to increase. The converging microstructural features point back to the original site of nucleation [4,11,12]. This is characteristic of some drop tube samples that undercool and solidify in free fall. If one extrapolates back along the elongated grains, one can see that nucleation occurred somewhere beyond the field of view in Figure 12 near the surface with no indication of other nucleation sites. This is to be contrasted with a sample of $NiAl_3$ from a previous study [4]. As can be seen in Figure 13, there are many nucleation sites in this sample as indicated by the multiplicity of dendrite orientations.

Some sample microstructures are more difficult to explain. Figure 14 compares microstructures of Pd, Ni, and Cu. The Pd and Cu samples illustrated were processed in the reducing H-He gas. The Ni sample was dropped in He. Examination of Figure 5 indicates that the conditions of processing are consistent with the reduction of surface oxides. The samples solidified completely in free fall and were greatly annealed. The large grains meet at a long meandering grain boundary, each sample appearing to have annealed to nearly one single large grain. A number of samples such as this were observed to fracture into two halves upon impact at the bottom of the drop tube, apparently fracturing along the long grain boundary.

One might ask how these samples could completely anneal to such a large grain size. After repeated polishing and careful re-etching it was possible to reveal the underlying microstructure of the Ni sample. Figure 15 illustrates the original dendritic solidification structure. As can be seen, the dendrite arm spacing has essentially the same dimension throughout the sample. Over the entire region of the one large annealed grain, the dendrites are all aligned in precisely the same orientation. In the region containing a few large annealed grains, the dendrites are somewhat misaligned from the rest of the sample. Since the dendrite arm spacing does not increase through the sample, solidification had to proceed more rapidly than the reheating from the release of the latent heat of fusion, implying extremely rapid solidification, very little if any thermal arrest due to solidification at the melting point, and probably very large undercooling, possibly hypercooling. One can notice the flattened side to the right in the region of several large grains due to the impact at the end of the drop tube. It is likely that the impact work hardened the sample, disrupting the original single crystal grain. The creation of these misaligned dendrites inhibited the annealing of the sample in this region. Since the sample was probably a single crystal prior to impact, only one nucleation event occurred. It is likely that the Pd and Cu samples from Figure 14 solidified under similar circumstances.

Since the only samples to exhibit the large annealed microstructures were processed under the reducing gas conditions favorable for oxide reduction, the data consistent with the conclusion that oxide surface films on the sample surface can contribute nucleation sites making it difficult to undercool molten samples in the drop tube environment.

Control of the atmosphere is not the only necessary condition for the suppression of nucleation. Most of the samples of Ni, Pd, nad Cu were processed under favorable nonoxidizing conditions, but many of the drops had many dendrite orientations, grains, and probable nucleation sites. This could be due to the additional requirement that a certain amount of time at elevated temperatures is necessary to remove surface oxides and/or dissolved oxygen on or in the sample. The few samples that exhibited large grain annealed structures with uniform dendrite arm spacings and orientations were also overheated prior to dropping. Pyrometer malfunctions caused the drop tube operator to greatly overheat these samples. This caused superheating of the samples and provided more time for reduction of the surface oxides, as well as dissolution of residual nuclei in the melt. These factors are known to favorably contribute to maximum undercoolings. Other studies with oxide glass formers indicate that superheating to as much as 350°C is required to achieve maximum undercoolings [13].

SUMMARY AND CONCLUSIONS

1) Electron beam melting of elemental metals in the form of wires was difficult to implement.

2) Electromagnetic levitation melted samples of Pd, Ni, and Cu processed in a vacuum were too large to completely solidify in the drop tube. This is due to their low melting temperature and insufficient radiation cooling rates.

3) Numerous samples contained dissolved gases, primarily oxygen. Upon sample cooling, the gas became less soluble and precipitated as porosity at the interdendritic spaces.

4) One can obtain microstructures indicative of large undercoolings, single nucleation events, and rapid solidification rates by containerless cooling in drop tubes.

5) Environmental conditions favorable for reduction of surface oxides are not the only necessary constraint for limiting nucleation in drop tubes.

6) Large superheatings are beneficial for undercooling from two standpoints. First, superheating aids the reduction of surface oxides already present on the sample surface. Second, superheating can aid the dissolution of residual nuclei in the molten metal. Therefore, superheatings are highly desirable for undercooling studies.

REFERENCES

1. Steinberg, J., Lord, A. E., Jr., Lacy, L. L., and Johnson, J.: Production of Bulk Amorphous $Pd_{77.6}Si_{16.5}Cu_6$ in a Containerless Low-Gravity Environment. Appl. Phys. Lett., Vol, 38, 1981, pp. 135-137.

2. Robinson, M. B.: Undercooling Measurement in a Low-Gravity Containerless Environment. M.S. Thesis, University of Alabama in Huntsville, 1981.

3. Lacy, L. L., Robinson, M. B., and Ratz, T. J.: Containerless Undercooling and Solidification in Drop Tubes. J. Crys. Growth, Vol. 51, 1981, pp. 47-60.

4. Ethridge, E. C., Curreri, P. A., and Kelly, M.: Results of the Technical Exchange Agreement Between NASA and DuPont on the Containerless Drop Tube Solidification of $NiAl_3$. NASA TM-86473, 1984.

5. Richardson, F. D., and Jeffes, J. H. E.: The Thermodynamics of Substances of Interest in Iron and Steel Making from 0°C to 2400°C. J. Iron Steel Inst., Vol. 60, 1948, pp. 261-270.

6. Kubaschewski, O., Evens, E. Li., and Alcock, C. B.: Metallurgical Thermochemistry, Pergamon Press, London, 1967.

7. Champion, F. C., and Davy, N.: Properties of Matter. Blackie and Son Limited, London, 1957.

8. Ethridge, E. C., Theiss, J., Curreri, P. A., and Abbaschian, G. J.: Electromagnetic Levitation Coil Fabrication Technique for MSFC Containerless Processing Facilities. NASA TM-82565, 1983.

9. Petzow, G.: Metallographic Etching. American Society for Metals, Metal Park, Ohio, 1978.

10. Fast, J. D.: Interaction of Metals and Gases. Vol. 1, Academic Press, New York, 1965.

11. Abbaschian, G. J., and Flemings, M. C.: Supercooling and Structure of Levitation Melted Fe-Ni Alloys. Met. Trans A., Vol. 14A, 1983, pp. 1147-1157.

12. Ethridge, E. C., Curreri, P. A., Kelly, M., Workman, G., Smith, A. M., and Bond, R.: Containerless Drop Tube Rapid Solidification and Grain Refinement of $NiAl_3$. Second Symposium on Space Industrialization, NASA CP-2313, 1984, pp. 293-303.

13. Ethridge, E. C., Curreri, P. A., and Pline, D.: Heterogeneous Nucleation and Glass Formation Studies of Gallia-Calcia. Submitted to J. Am. Ceramic Soc. 1986.

TABLE I. PROPERTIES OF METALS MELTED BY THE PENDANT DROP TECHNIQUE

Metal	Melting Temperature (°C)	Density (g/cc)	Surface Tension (dyne/cm)	Wire Diameter (cm)	Critical Mass (mg)	Critical Length (cm)
Platinum	1769	21.4	1800	0.0127 0.025	73.3 144.3	27.0 13.7
Rhodium	1966	21.0	2000	0.0127 0.025	81.4 160.3	30.6 15.5
Rhenium	3180	12.4	2700	0.0127 0.025	109.9 216.4	70.0 35.5
Iridium	2454	22.5	2250	0.0127 0.025	91.6 180.3	32.1 16.3

TABLE II. SUMMARY OF DROP TUBE SPECIMENS

LEGEND: pee: picture, electroetched pe: picture, chem. etched pr: picture, real surface(light micros.) sem: scanning electron micrograph C: cooling curve

NT221	Rh	High purity, electron beam, pee
NT224	Rh	High purity, e beam, mounted, not etched
NT227	Rh	High purity, e beam, mounted, not etched
NT228	Rh	High purity, e beam, mounted, not etched
NT269	Pd	High purity, pee
NT314	Cu	electrical wire, test drop,no sample,P/C
NT339	Cu	electrical wire, vacuum, test drop,not mounted, splat on valve
NT344	Cu	High purity 1mm wire, 200T 5.75% HeH atmos. quenched into Al foil, pe
NT345	Cu	High purity wire, lost sample, C
NT346	Pd	wt bef 336.4mg, arced, 200T Ar in bell jar, 200T HeH in tube, splat, not mounted
NT349	Cu	High purity, HeH atmos, C
NT351	Cu	High purity, HeH tube, Ar in bell jar, pyro 1250 C, dirty, pe
NT357	Cu	bell jar-200T Ar, 200T HeH tube, catch area-air, P/C
NT417	Pd	wt bef 316.99mg, wt aft 316.43mg, 200T He, pe
NT420	Pd	wt bef 338.63mg, wt aft 321.25mg, pe
NT422	Pd	wt bef 190.83mg, 200T He, prepump to 6x10-5, splat
NT423	Ni	wt bef 252.91, 200T He, prepump to 7x10-5, not mounted
NT426	Ni	wt bef 252.73mg, wt aft 252.81mg, He atmos, prepump to 9.8x10-4, not fully melted, pr,pe, sem
NT427-8	Ni	wt bef 250.0 mg, wt aft 248.03mg, He atmos, prepumped to 8x10-5, not fully melted, pe
NT429	Ni	wt bef 358.74mg, 200T He, prepumped 5x10-5, no melt, no sample
NT430	Ni	wt bef 393.29mg, 200T He, prepump to 1x10-4,no sample
NT434	Cu	HeH atmos, not total melted, pe
NT435	Cu	HeH atmos, not total melted, pe
NT446	Ni	wt bef 299.48mg, wt aft 300.0mg, 200T HeH atmos, prepump to 5x10-5, 6kv to lev, 5.2kv to melt, pe, C
NT447	Ni	wt bef 300.15mg, wt aft 300.16mg, 200T HeH atmos,prepump to 6x10-5, 6kv to lev, 5kv to melt, sem, pe, C
NT448	Ni	wt bef 213.43mg, wt aft 213.57mg, 200T HeH atmos, prepump to 6x10-5, 5.3kv to melt, rainy day, sem, pe
NT449	Ni	wt bef 294.28mg, wt aft 294.47mg, HeH atmos, prepump to 7.4x10-6, rainy day, 5.1kv to melt, sem, pe
NT450	Pd	wt bef 335.36mg, wt aft 334.12mg, HeH atmos, prepumped to 5x10-5, rainy day, 4.6kv to melt fully, pe, sem
NT451	Pd	wt bef 351.61mg, HeH atmos, prepump to 4x10-5, rainy day, splat
NT452	Pd	wt bef 371.32mg, HeH atmos, prepump to 8x10-5, rainy day, sample fractured in half, pe
NT453	Ni	wt bef 358.74mg, wt aft 360.0mg, 760T air, 6kv lev, 3.8kv melt, pe, C*
NT454	Ni	wt bef 350.0mg, wt aft 342.94mg, 760T air, 6kv lev, 3.7kv melt, pe, C
NT455-6	Ni	wt bef 295.9mg, wire knot, no lev in 760T air
NT457	Cu	High purity, air splat, 6kv lev, 5.8 melt, C
NT458	Cu	760T air splat, C
NT459	Pd	wt bef 360.5mg, 760T air, 6kv lev, 5.9kv melt, pr, pe, sem
NT460	Pd	wt bef 372.88mg, 760T air, 6kv lev/melt, pe, C
NT461	Pd	wt bef 387.77mg, 760T air, 6kv lev/melt, pr, pe, sem
NT462	Pd	wt bef 393.32mg, 760T air, 6kv lev/melt, pe
NT463	Cu	760T air splat, C
NT464	Cu	760T air splat, C
NT465	Cu	splat in vacuum, 3.8x10-5 T, 6kv lev/melt, C

TABLE II. (Concluded)

NT466	Cu	1mm wire, lost sample in tube
NT468	Pd	wt bef 263.36mg, 9x10-5 vacuum, splat, C
NT469	Pd	wt bef 311.23mg, 200T HeH atmos, prepump to 4x10-5, 6kv lev, 5.1 melt, pe
NT470	Pd	wt bef 323.39mg, HeH atmos, prepump to 8x10-5, 6kv lev, 4.8kv melt, pe
NT472	Cu	HeH atmos, prepump to 4x10-5, one end only melted, pe
NT474	Cu	High purity, 200T HeH atmos, prepump to 8x10-5, 6kv lev, 4.8kv melt, pe
NT559	Ni	wt bef 374.03mg, 8x10-5 T vacuum, pe, C*
NT560	Ni	wt bef 285.24mg, 2x10-4 T vacuum, sem, pe, C*
NT577	Cu	wt bef 240.14mg, wt aft 238.78mg, 500T HeH atmos, prepump to 9x10-5, incomplete melt, not mounted
NT578	Cu	wt bef 232.25mg, wt aft 230.8mg, 400T HeH atm, prepump to 6x10-5, fell from coil, not mounted
NT581	Cu	wt bef 244.30mg, wt aft 240.31mg, 300T HeH atmos, prepump to 7x10-5, not mounted
NT582	Cu	wt bef 189.10mg, wt aft 185.98mg, 300T HeH atmos, prepump to 9x10-5, C?
NT583	Cu	wt bef 184.89mg, 183.07mg, 300T HeH atmos, prepump to 9x10-5, not mounted
NT584	Cu	wt aft 268.30mg, HeH atmos, not high purity, test drop, not mounted
NT585	Cu	wt aft 231.77mg, 150T HeH atmos, prepump to 5x10-4, half splat, data as NT584
NT586	Cu	wt aft 223.17mg, 150T HeH atmos, prepump to 5x10-4, elongated half splat, test
NT587	Cu	wt bef 177.89mg, wt aft 176.14mg, 150T HeH atm, prepump to 8x10-5, incomplete melt, not mounted
NT589	Ni	wt bef 371.30mg, wt aft 371.00mg, 150T HeH atmos, prepump to 8x10-5
NT590	Ni	wt bef 380.74mg, wt aft 380.47mg, 150T HeH atmos, prepump to 8x10-5
NT591	Pd	wt bef 269.02mg, wt aft 258.51mg, 150T HeH atmos, prepump to 8x10-5, pe
NT592	Pd	wt bef 196.76mg, wt aft 189.19mg, 150T HeH atmos, prepump to 5x10-5, pe
NT594	Cu	wt bef 163.73mg, wt aft 162.54mg, 150T HeH atmos, prepump to 9x10-5, not levit, not mounted
NT620	Pt	e beam, 5x10-5 vacuum
NT624	Pt	e beam, 5x10-5 vacuum, W stinger, pee, C
NT625	Rh	e beam, 2x10-5 vacuum, W stinger, no data, pee
NT626	Pt	e beam, 4x10-5 vacuum, lost, C
NT627	Pt	e beam, 4x10-5 vacuum, not complete melt, not mounted, C
NT630	Pt	e beam, 6x10-5 vacuum, pee
NT656	Pt	e beam, 24cm wire @ .125"
NT657	Pt	e beam, no data, wt aft 65.4mg, may be good melt
NT658	Pt	e beam, .125" wire, 5x10-5 vacuum
NT659	Pt	e beam, not mounted, wt aft 50.23 mg, .127" wire in sample, C
NT660	Pt	e beam, .127" wire, 4x10-5 vacuum
NT661	Pt	e beam, no data, not mounted, wt aft 24.28 mg
NT662	Rh	e beam, .127"wire, wt aft 20.61 mg, irregular shape, may have wire in it, C
NT663	Pt	e beam, .127"wire, wt aft 59.3mg, wire embedded in it, C
NT664	Rh	e beam, wt aft 23.2mg, .127" wire embedded in it, C
NT665	Rh	e beam, wt aft 30.7mg, may have wire embedded
NT670	Ir	e beam, .25" wire, 5x10-5 vacuum, wt aft 76.81mg, wire embedded
NT671	Ir	e beam, .25" wire, 5x10-5 vacuum, wt aft 33.92mg, wire may be embedded

TABLE III. OBJECTIVES AND MAGNIFICATIONS ON THE ZEISS MICROSCOPE

Objective	Magnification
2.5/0.08	40
4.0/0.10	65
16/0.035	260

TABLE IV. NORMALIZED MASS SPECTROMETRY DATA FOR AIR

Mass	Species	Normal Partial Pressure (torr)	Mass Spec. Data (torr)	Ratio (Pressure: Mass Spec.)
1	H^+	0.0004	4.0E-9	1.0E5
4	He^+	0.004	1.5E-11	2.7E8
16	O^+		6.0E-8	
17	OH^+			
18	H_2O^+	0.2 to 43	9.0E-8	
20	Ar^+	7.068	1.0E-8	7.1E8
28	N_2^+	593.4	6.5E-6	9.1E7
32	O_2^+	159.2	1.5E-6	1.1E8
40	Ar^+		9.5E-7	
44	CO_2^+	0.228	1.2E-7	1.9E6
		756 to 799	9.25E-6	

TABLE V. SOLUBILITIES OF N_2, H_2, AND O_2 IN THE METALS

Metal	Solubility of H_2	Solubility of O_2	Solubility of N_2
Cu liquid	0.03 a/o	unlimited solubility, eutectic at 1065°C and 0.86 a/o	insoluble
Cu solid	0.009 a/o	0.04 a/o	insoluble
Ni liquid	0.1 a/o	unlimited solubility, eutectic at 1438°C and 0.04 a/o	insoluble
Ni solid	0.2 a/o	0.04 a/o	insoluble
Pt liquid	?	?	insoluble
Pt solid	0.016 a/o	?	insoluble
Pd liquid	0.7 a/o	? PdO decomposes at 750°C	insoluble
Pd solid	0.4 a/o	0.63 a/o	
Rh liquid	very low	Rh_2O_3 decomposes at 1100°C	insoluble
Rh solid	very low	"considerable insolubility"[a]	insoluble

a. Fast, 1965.

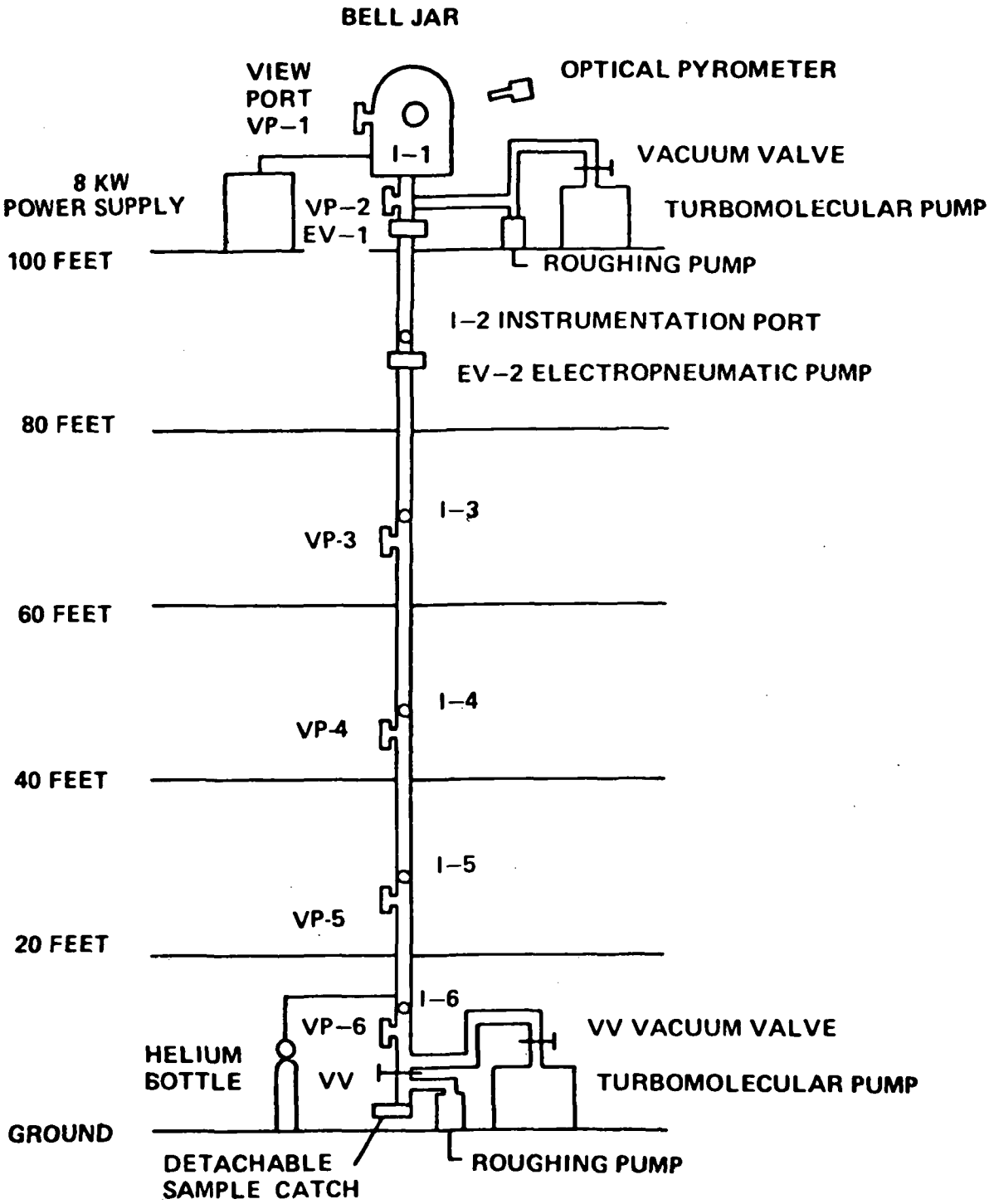

Figure 1. Schematic diagram of the MSFC drop tube.

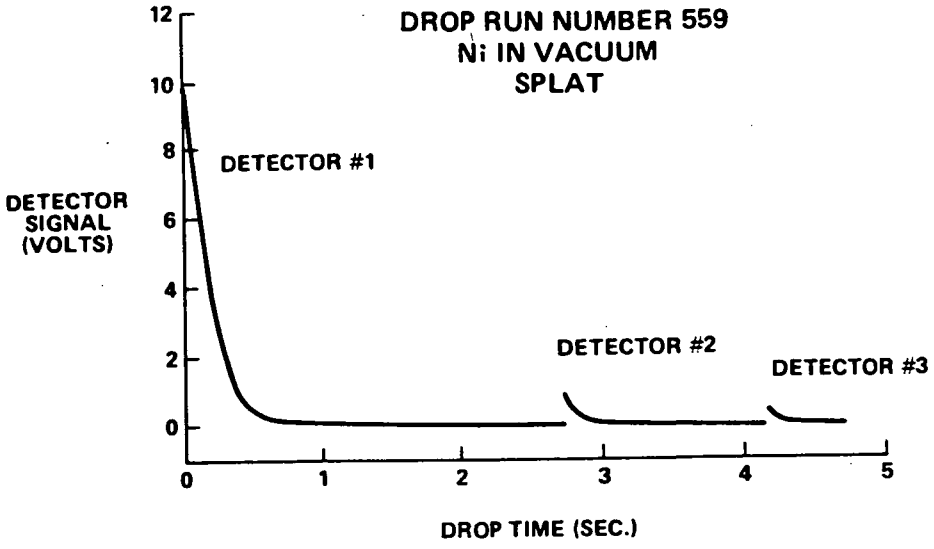

Figure 2. Example of recalescence detector data.

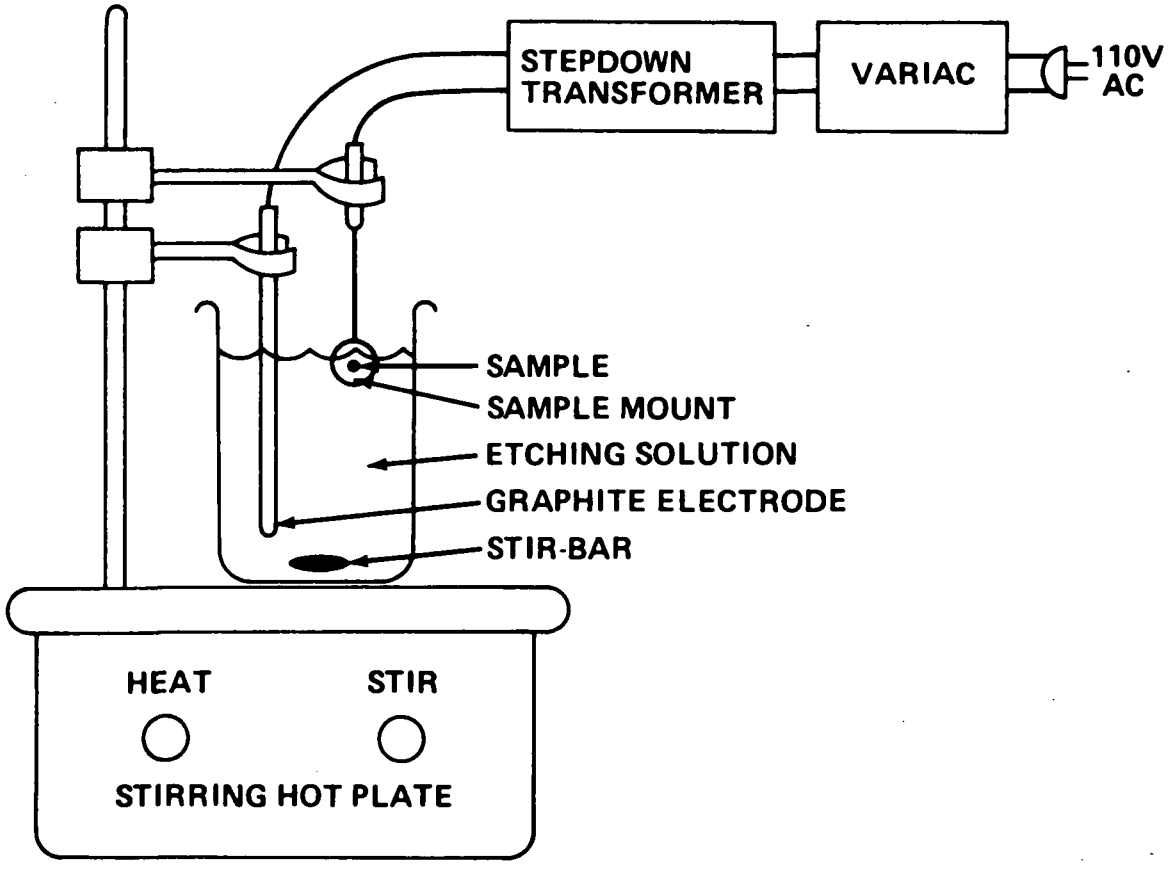

Figure 3. Schematic diagram of the electrochemical etching apparatus.

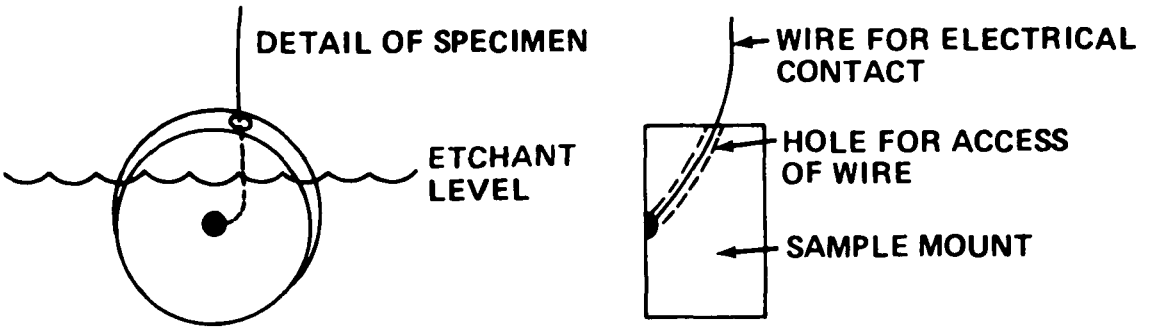

Figure 4. Illustration of the procedure for making electrical contact to the sample for electrochemical etching.

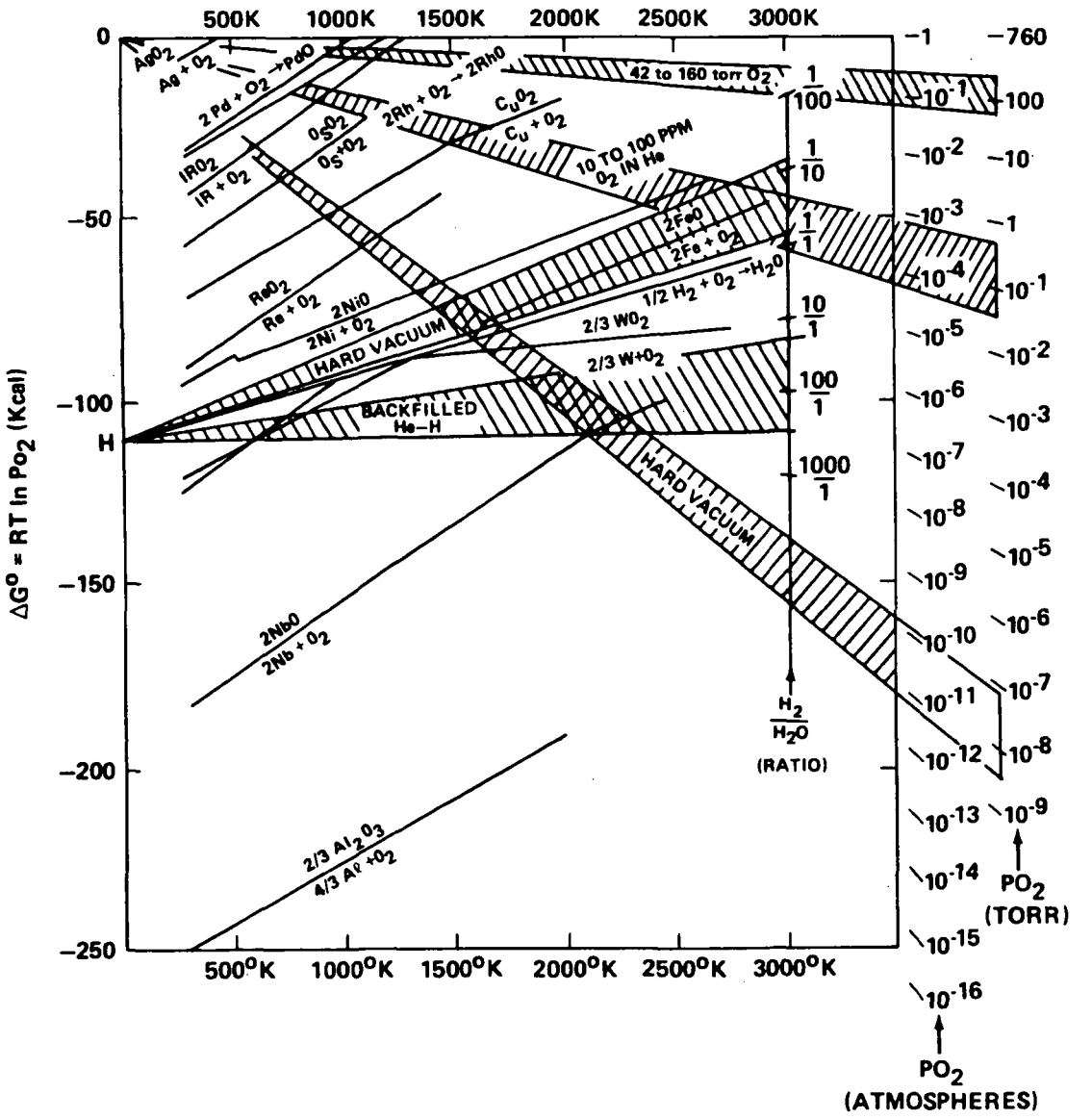

Figure 5. Ellingham diagram for oxide stability curves.

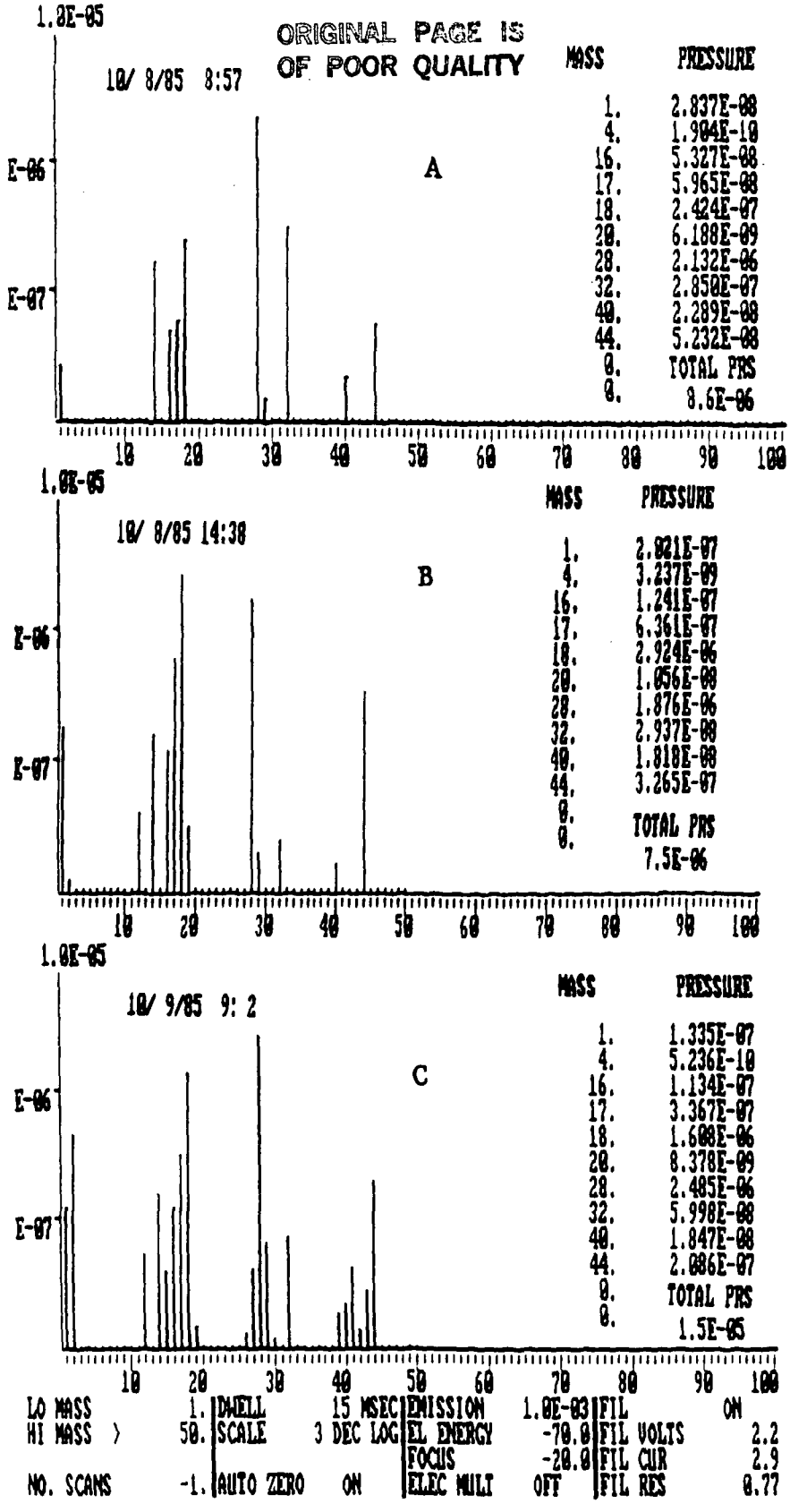

Figure 6. Mass spectrometry data for hard vacuum conditions.

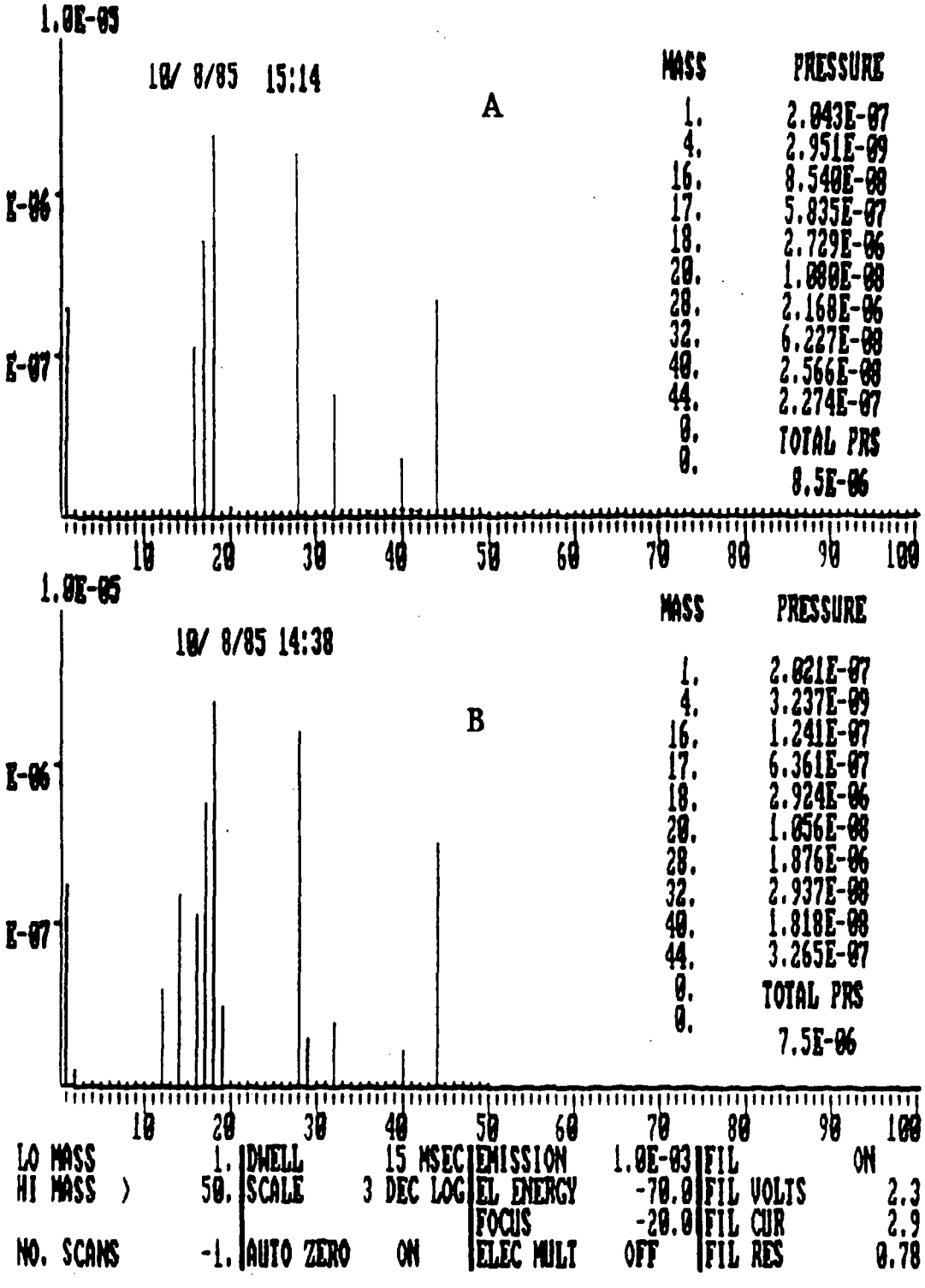

Figure 7. Mass spectrometry data before and after electron beam furnace operation.

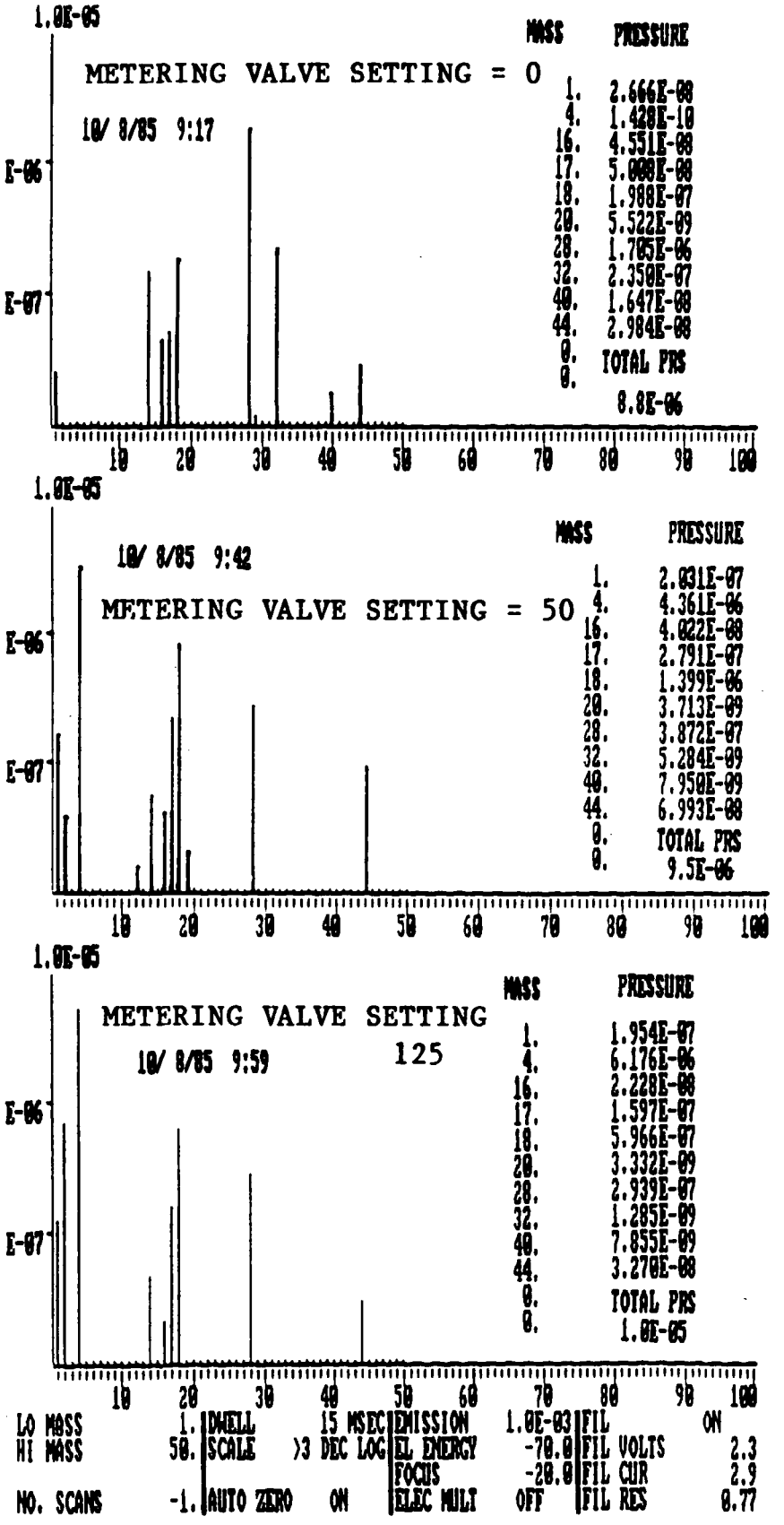

Figure 8. Mass spectrometry data for three different metering valve settings sampling 200 torr H-He.

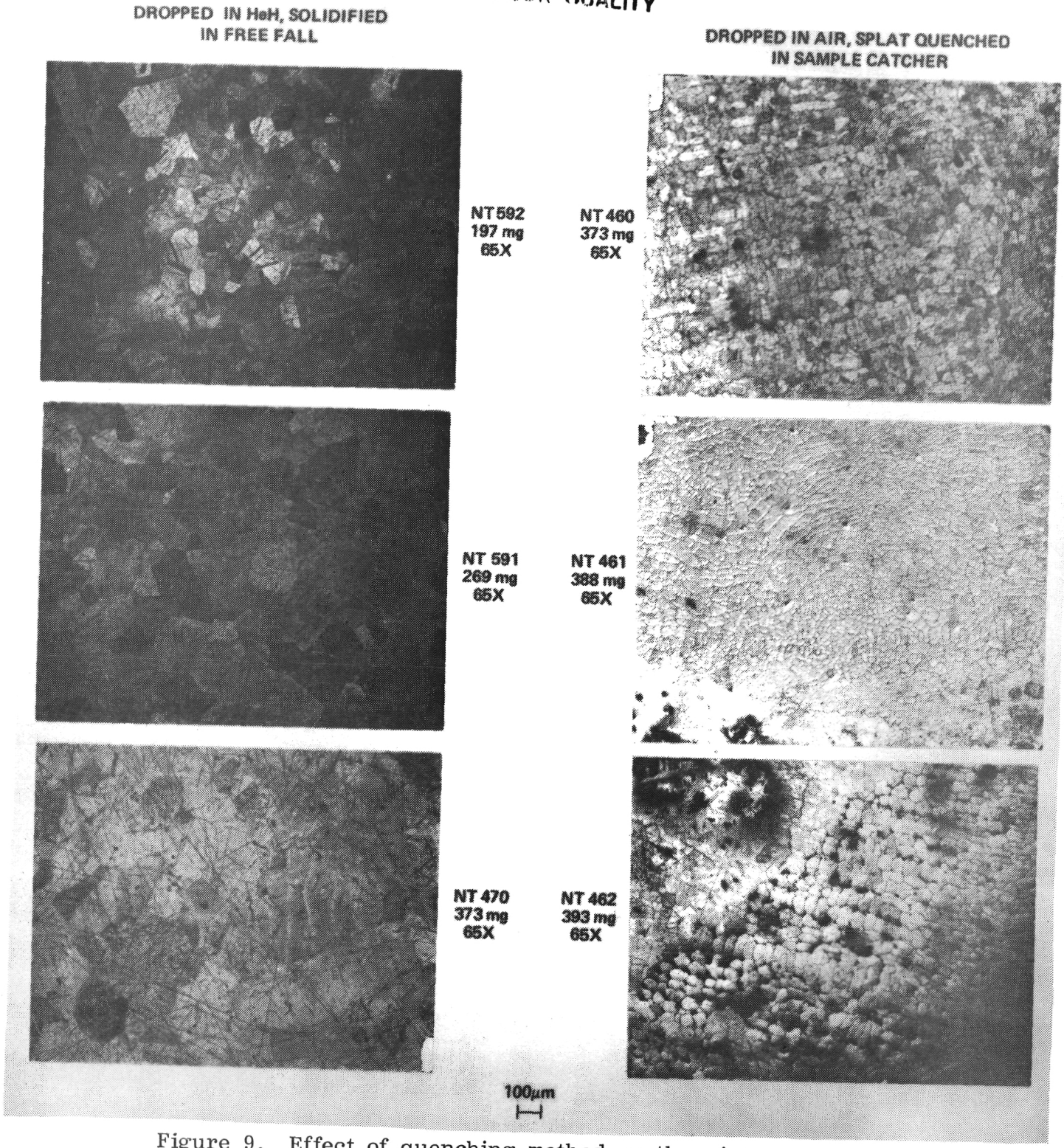

Figure 9. Effect of quenching method on the microstructure of palladium.

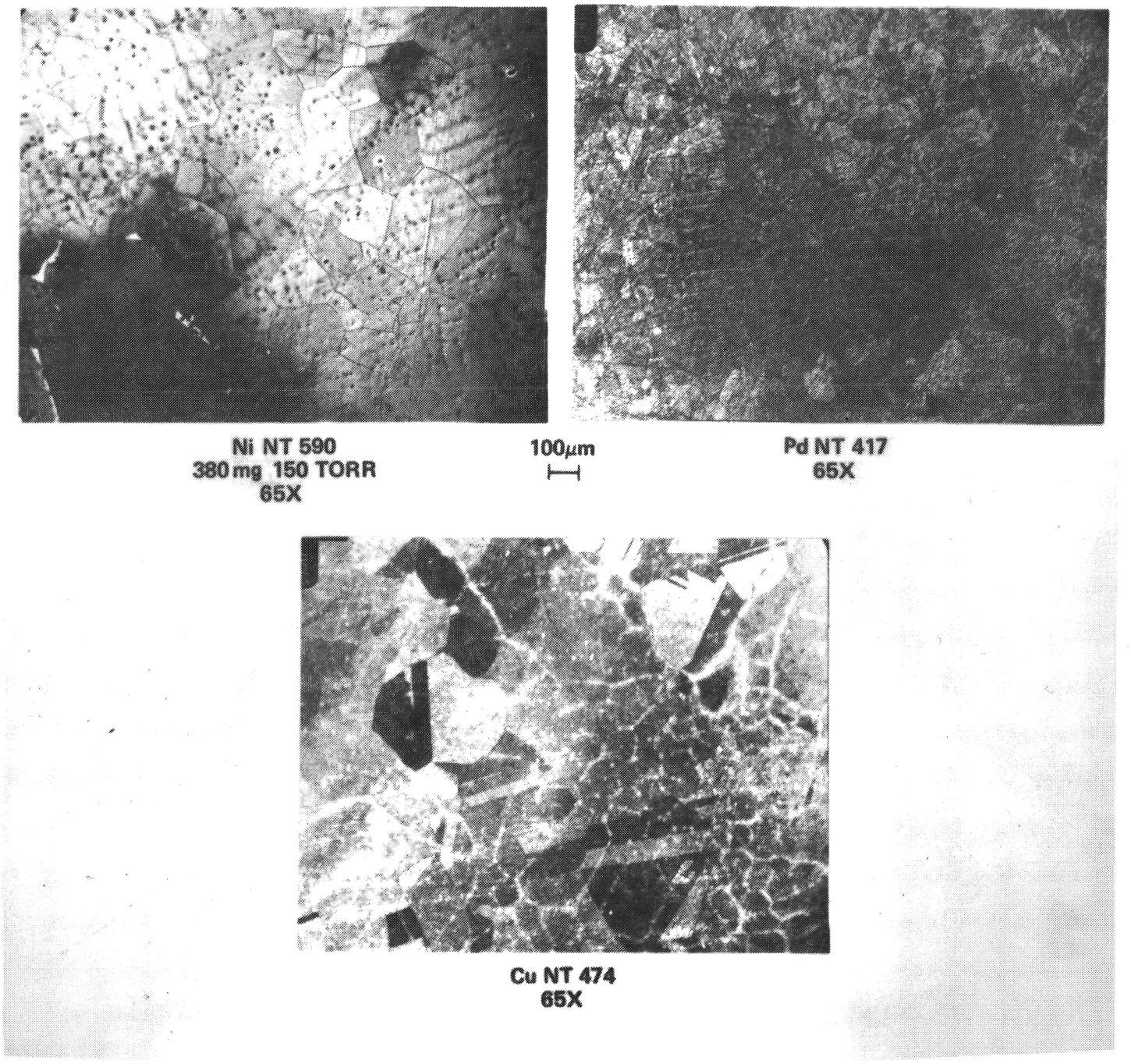

Figure 10. Self annealed microstructures with underlying dendritic solidification microstructure revealed by etching.

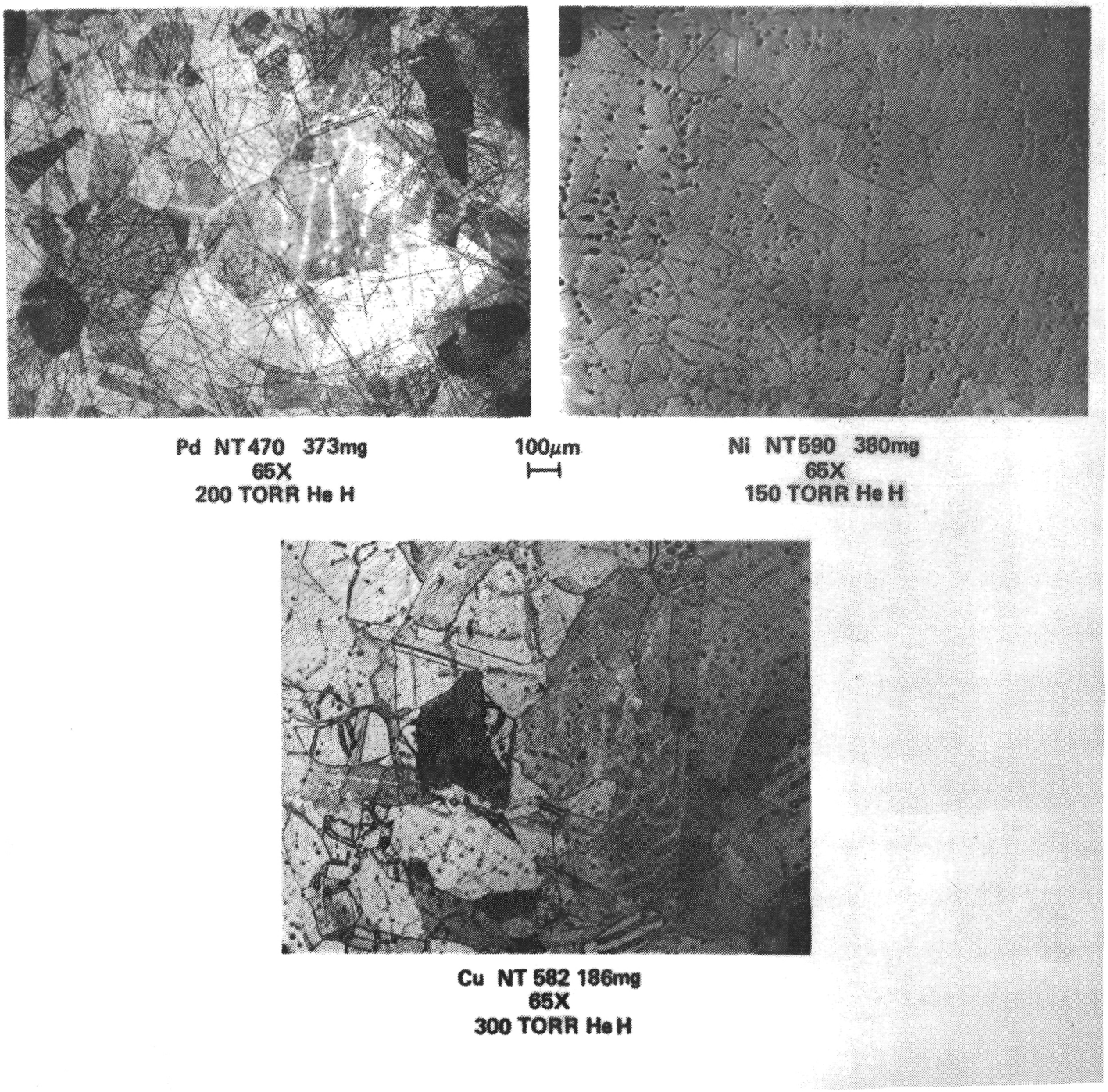

Figure 11. Self annealed microstructures with underlying dendritic solidification microstructure revealed by interdendritic porosity.

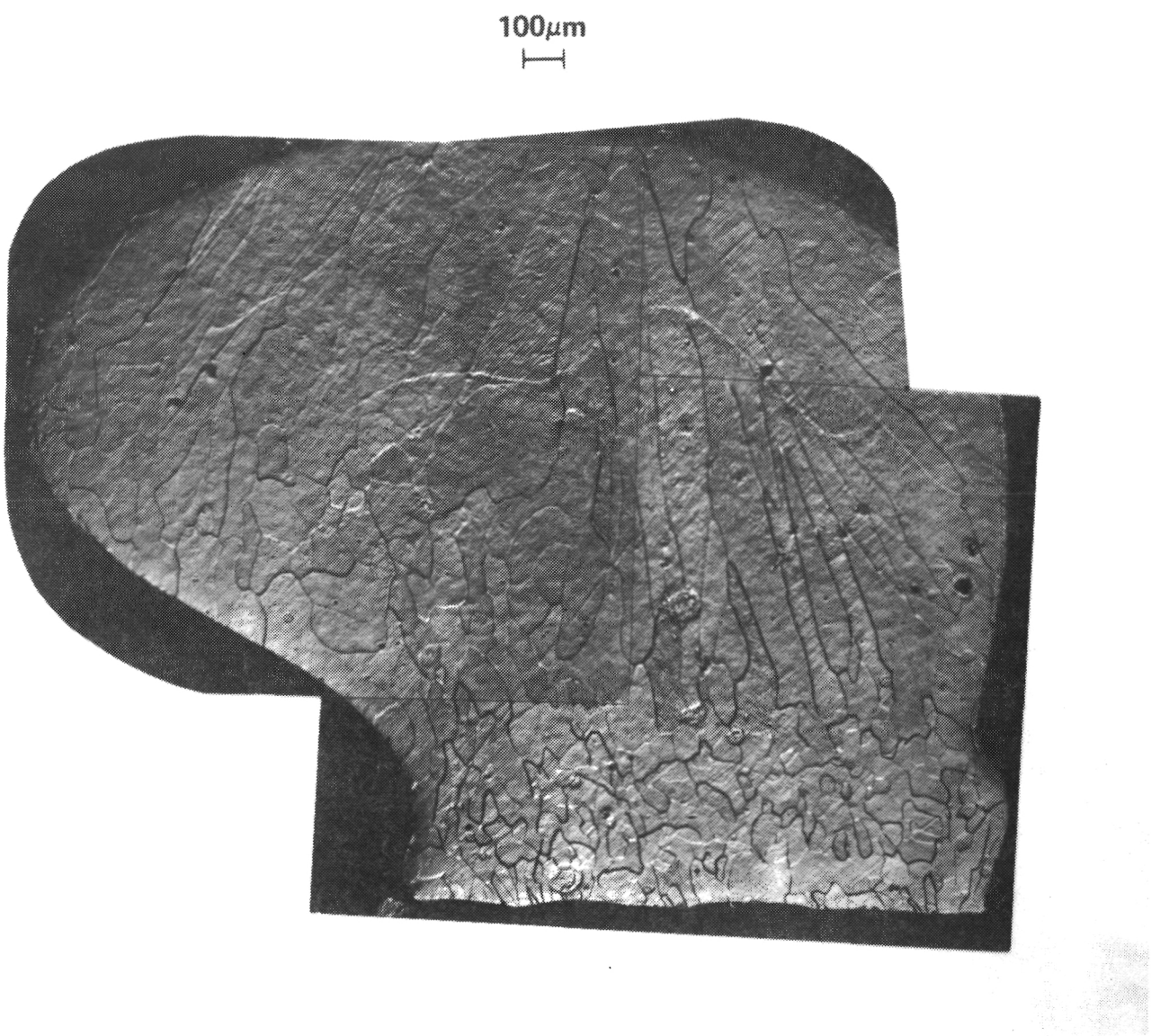

Figure 12. Composite micrograph of a Cu sample partially solidified in free fall.

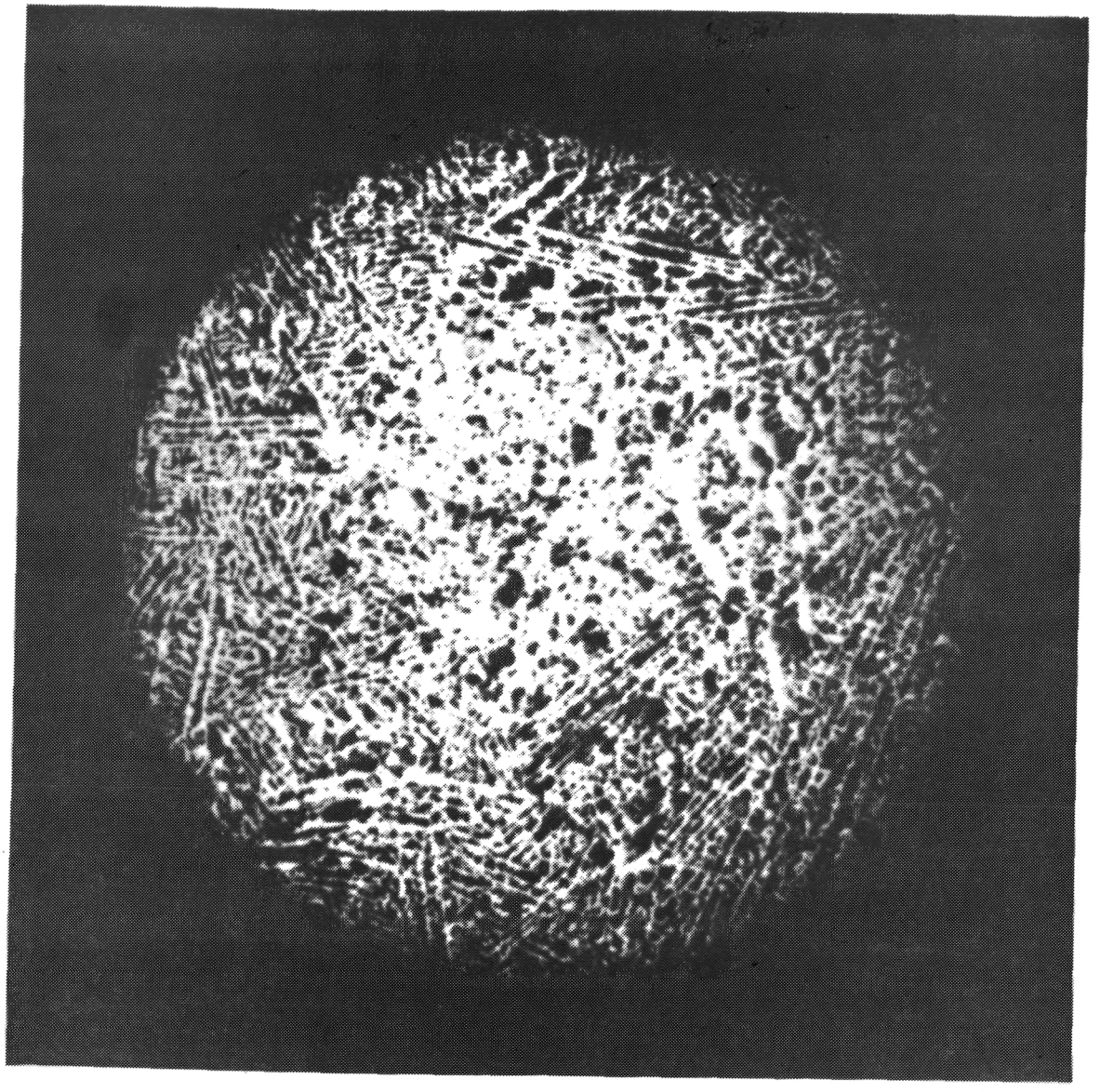

Figure 13. Micrograph of $NiAl_3$ illustrating numerous nucleation sites and multiplicity of dendritic arm orientations.

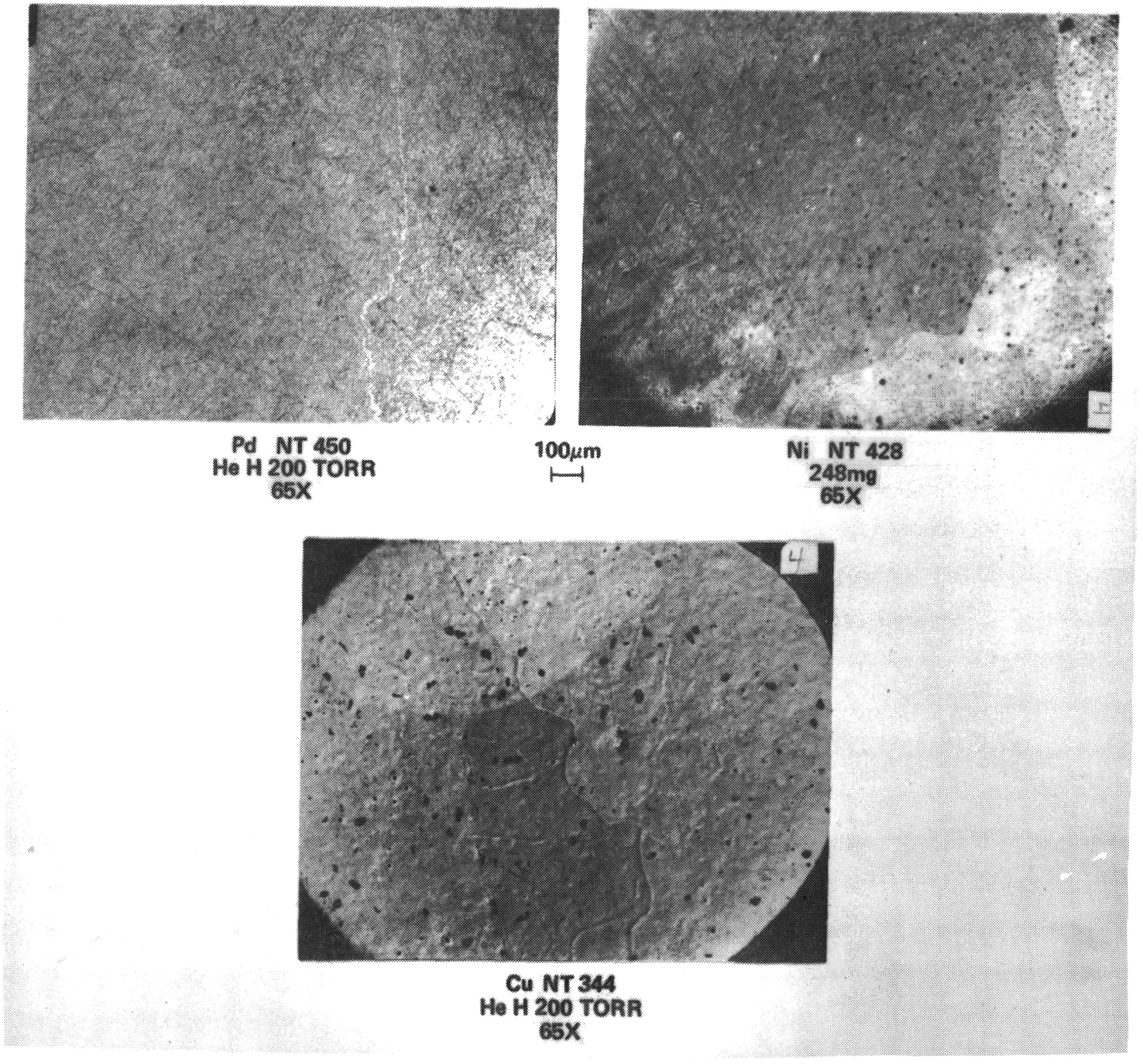

Figure 14. Micrographs of Pd, Ni, and Cu samples with very large annealed grain size.

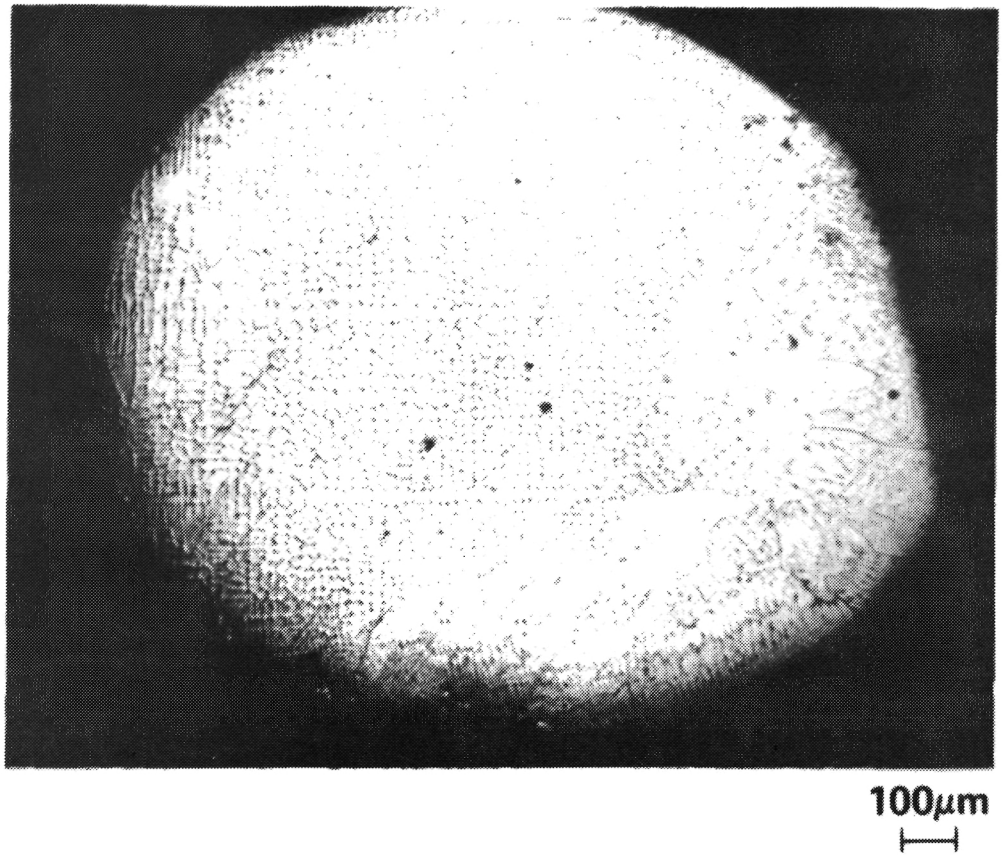

Figure 15. Micrograph of large grain size Ni sample with underlying dendrites revealed.

APPROVAL

SURFACE FILM EFFECTS ON DROP TUBE UNDERCOOLING STUDIES

Center Director's Discretionary Fund Final Report

By E. C. Ethridge and W. F. Kaukler

The information in this report has been reviewed for technical content. Review of any information concerning Department of Defense or nuclear energy activities or programs has been made by the MSFC Security Classification Officer. This report, in its entirety, has been determined to be unclassified.

A. J. DESSLER
Director, Space Science Laboratory

☆U.S. GOVERNMENT PRINTING OFFICE 1986–631-058/20133